Proceedings World Geothermal Congress 2005
Antalya, Turkey, 24-29 April 2005

Modeling Silica Deposition in a Porous Medium Column

Sutopo

Geothermal Lab., Dept. of Petroleum Eng., Institut Teknologi Bandung (ITB), Jl. Ganesha 10 Bandung 40132, Indonesia

sutopo@tm.itb.ac.id

Key Words: Silica deposition, numerical modeling

ABSTRACT

The transport of minerals in hot water reservoirs has received considerable attention because of its importance in geothermal resources development. In the past, numerical techniques have been employed to obtain solutions to silica transport and deposition problems. A fully implicit numerical model, which describes the permeability decrease caused by the silica deposition in porous medium, has been formulated and applied to simulate the laboratory experiments and filed data. A finite difference method is used to discretize the mass of water, silica reaction, and energy balance equations. As an expression for silica deposition rate, we used models of Ramstidt and Barnes.

The numerical model of the rate of silica deposition was applied to the experimental results obtained by Itoi *et al*. The experiments involved an isothermal flow through packed columns. The rate constant of Ramstidt and Barnes was used in this calculation. A good agreement in the changes of flow rate, permeability, specific deposit, and pressure was achieved.

1. INTRODUCTION

The transport of chemical in the hot water reservoirs has received considerable attention because of its importance in geothermal resources development. One of the problems associated with using hot water from the reservoirs is the inevitable deposition of chemical as exploitation proceeds. Deposition or scaling occurs not only in the surface equipment but also in the immediate vicinity of the well bore. Scale composed of silica, calcite or anhydrite is encountered in exploited reservoirs throughout the world.

Amorphous silica heads the list of the precipitates associated with the injection of wastewater. Deposition of silica around the wellbore causes reduction in formation permeability and subsequently the injectivity of the well (Itoi et al. 1987, 1989).

The primary objectives of this work are to develop a fully implicit numerical model, which describes the porosity and permeability decrease caused by the silica deposition in porous medium, and to apply the model to the laboratory experiments data.

A finite difference method is used to discretize the mass of water, silica reaction, and energy balance equations. Time is discretized as fully implicit, to ensure the numerical stability. The model employs upstream weighting to calculate the interface of water enthalpy and silica concentration, harmonic weighting for intrinsic permeability, and an arithmetic average for the mass density and viscosity. The nonlinear balance equations are linearized using a residual-based Newton-Raphson iterative technique. We used models of Ramstidt and Barnes (1980) for silica deposition rate.

2. SILICA DISSOLUTION/PRECIPITATION

2.1 Silica Solubility

Silica occurs in a number of different forms including quartz, cristobalite, tridymite and amorphous silica. All of these various polymorphs are known to occur in the nature. In study of hydrothermal system, quartz and amorphous silica are the two polymorphs most commonly encountered.

It is generally accepted that silica water reaction is a simple surface reaction given by

$$SiO_{2(s)} + 2H_2O \Leftrightarrow Si(OH)_{4(aq)} \quad (1)$$

Recently, Rimstidt (1997) published new quartz solubility measurements in pure water that approached equilibrium from undersaturation at 21, 50, 74, and 96 ^{o}C. He showed a solubility function correlated for temperature range 0 to 300 ^{o}C:

$$\log\ m = -1107.12/T_K - 0.0254 \quad (2)$$

where m is the molal solubility of quartz and T_K is temperature in Kelvins.

2.2 Kinetics of Silica Reaction

As the geothermal is extracted and steam is separated, the remaining water fraction becomes highly supersaturated with respect to amorphous silica. Amorphous silica deposition may then occur, at a rate which appears to be governed by several factors such as degree of supersaturation, temperature, pH, presence of dissolved salts and foreign ions, availability of nucleating species, and fluid regime. Deposition is known to occur by direct deposition on solid surfaces (heterogeneous nucleation) or by polymerization followed by colloidal deposition (homogenous nucleation).

There are number of experimental studies made on the kinetics of amorphous silica polymerization which have mostly measured the disappearance of monomer silica during the course of the reaction (Rimstidt and Barnes, 1980; Bolmann et al., 1980; Carroll et al., 1998; Tester et al., 1997). The kinetics of polymerization are so complex that the studies yielded various estimates of the order of reaction. The following discussion covers the important kinetics models of silica deposition, which will be used in this work in modeling silica transport in geothermal reservoirs.

Rimstidt and Barnes (1980) performed their experiments in salt-free water and derived the kinetics of silica dissolution precipitation at temperatures 0 to 300 ^{o}C. Their rate equation can be expressed as

$$R_c = -k(C - C_s) \quad (3)$$

where $k = k^{-}\frac{A}{M}$

Here, k^{-} is the dissolution constant, *A/M* is the ratio of the relative surface area to the relative mass of water in the system. *C* is the silicic acid concentration (mg/kg), and C_s is the saturation concentration of the silica phase present. The Surface area *A* is a function of the shape of particles and the degree of fracturing. They also concluded that the rate constant for precipitation of all silica phases is the same and can be expressed as

$$\log k^{-} = -0.707 - \frac{2598}{T_K} \quad (4)$$

where T_K is temperature in Kelvins.

Bohlmann et al. (1980) studied molecular deposition from controlled synthetic solution. They monitored the deposition of monosilicid acid flowing through a column packed with granular amorphous silica and other similar forms. They found that after the substrate was coated fully with amorphous silica, the nature of the substrate had no effect on the deposition rate of silica but an increase in salt concentration to 4.0 molal increases the deposition rate by more that an order of magnitude. Fleming (1986) studied silica polymerization (without nucleation) in an attempt to resolve conflicting results on the reaction order. His experiments were performed at 25-50 ^{o}C, 0-1 molal NaCl and pH from 4 to 8 in unbuffered solutions. Based on the results of his differential rate data plus other experimental results (Bohlmann et al., 1980), he suggested two kinetics regimes for silica polymerization.

In general form (Steefel and Lasaga, 1994), the rate of growth or dissolution of a mineral in water solution can be expressed as

$$R_c = \frac{A}{V}k\left(\frac{Q}{K} - 1\right) \quad (5)$$

and, $k = k_{25}\exp\left[\frac{-E_a}{R}\left(\frac{1}{T_K} - \frac{1}{298.15}\right)\right]$

where, k_{25} is the reaction rate constant at 25 ^{o}C (4.30×10^{-14} moles m^{-2} s^{-1}), E_a is the activation energy (75.0 kJ/mol), *A/V* is the area over which the reaction occurs per unit volume of fluid (m^2/m^3), T_K is the temperature in ^{o}K, *R* is the gas constant (8.31456 J/mol K), *Q* is the activity of aqueous SiO_2, and *K* is the equilibrium constant for dissolution of quartz reaction.

Dove (1994) developed a new general expression for the dissolution kinetics of quartz from a compilation of published rate measurements and new hydrotermal data. The equation was based upon a surface reaction model that correlates changes in modeled surface complexes with quartz reactivity in aqueous solutions. The model was fitted to 271 independent measurements dissolution rate and quantifies reaction kinetics with temperature range from 25 to 300 ^{o}C for solution pH of 2 to 12 and 0 to 0.3 molal sodium. Tester et al., (1994) performed their experiments for quartz dissolution kinetics in pure water at temperature 25 to 625 ^{o}C from five different experimental apparatuses. Renders et al. (1997) carried out experiments to measure the rate of dissolution and precipitation for cristobalite (xtb) at temperature 150 to 300 ^{o}C. They derived the kinetics equations in a manner similar to that described by Ramstidt and Barnes (1980).

Carroll et al. (1998) investigated amorphous silica precipitation behavior in simple laboratory experiments and more complex filed experiments in the Wairaki, New Zealand, geothermal area. They found, in simple laboratory solution supersaturated with the absence of chemical impurities, the precipitation rate have a first-order dependence on $f(\Delta G_r)$.

Itoi et al. (1984) performed an experimental study involving near-isothermal flow of hot water sampled from the Otake geothermal field with supersaturated silica through a porous medium column. Their experimental results show that the silica scale is deposited mainly in the region near entry of the column, resulting in drastic permeability reduction. Based on the experimental results they obtained, Itoi at al. (1985) developed a one-dimensional mathematical model to represent silica deposition. The deposition model they considered takes into account the possible effect of aluminum on silica deposition. They also used the Kozeny-Stain equation to model the permeability reduction in the column. They were able to model the observed changes in flow-rate, specific deposit and permeability by using a very small inlet silica concentration. Itoi et al. (1986) extended the one-dimension model they used earlier to radial flow coordinates in order to predict changes in permeability and injectivity around a well. They assumed the reservoir is porous and radially symmetric with a homogenous thickness. In this model, the effect of trace metals (aluminum) on the silica deposition was neglected because rock fragments were used in their experiments instead of the aluminum beads. The equations used were also modified to represent the rapid decrease in permeability of column at early stages of their experiments. More recently, Itoi et al. (1987) modeled the decrease in injectivity of some wells in the Otake geothermal field. They used the radial flow model (Itoi et al., 1986a) but simplified the rate equation for silica deposition. A very small inlet silica concentration was also used in the model.

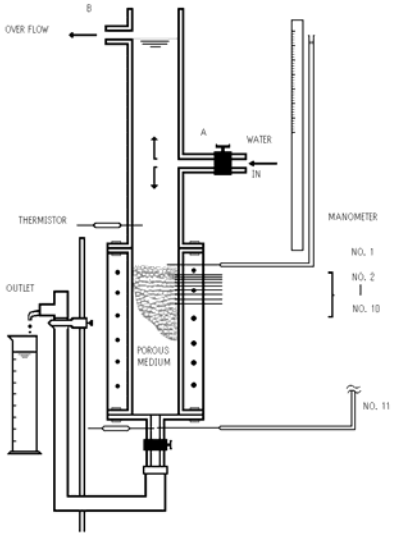

Fig. 1 Schematic view of the experimental tower (Itoi et al., 1984, 1986)

Itoi et al. (1984, 1986) studied the deposition of amorphous silica in porous column (50 cm long and 5 cm in diameter).

The schematic experiment is shown in Fig. 1, and the experiment conditions are given in Table 1. In their experiments a sample of hot water from the Otake geothermal field was introduced at a constant temperature 90 – 92 ^{o}C, into a column packed with aluminum beads. The column was operated at a constant pressure drop and changes in flow rate (due to deposition) were monitored. The amount of silica deposited in the column was then determined after drying the beads. They found that the most of silica scale was deposited within the first 10 cm of the porous medium. Their analysis showed that the permeability of the uppermost part of the porous column decreased by an order of two compared with its initial value, whereas in the deeper portions its change was insignificant. The amount of the silica deposit decreased rapidly with depth and progressively increased when the flow rate was increased.

Table 1 Summary of experimental conditions

Run No.	Total Hydraulic Potential (cm)	Initial Flow rate (cm^3/s)	Porosity	Filling Material	Silica Conc. (ppm)
RUN-1	52.4	63.9	0.40	BEAD	
RUN-2	24.0	38.8	0.39	BEAD	
RUN-3	15.4	29.0	0.40	BEAD	
RUN-4	31.9	45.6	0.40	BEAD	522
RUN-5	23.7	40.4	0.40	BEAD	522
RUN-6	19.3	34.3	0.39	BEAD	522
RUN-30	32.2	45.5	0.38	BEAD	493
RUN-31	30.7	50.4	0.48	ROCK	493
RUN-32	44.4	58.3	0.49	ROCK	493
RUN-33	39.1	54.1	0.39	BEAD	493
RUN-37	30.7	48.3	0.37	BEAD	475
RUN-38	30.7	44.8	0.49	ROCK	475
RUN-39	21.2	41.8	0.52	ROCK	475
RUN-40	39.8	62.9	0.48	ROCK	475

2.3 Mathematical Model of Silica Deposition

In the past, numerical techniques have employed to obtain solutions to silica transport and deposition problem (Lai et al., 1985; Itoi at al., 1985, 1986a, 1986b, 1987; Verma and Pruess, 1988; Wells and Ghiorso, 1991; Malate and O'Sullivan, 1992, 1992a, 1993; Lowell et al., 1993; Steefel and Lasaga, 1994; Canals and Meunier, 1995; White, 1995, 1997; Bolton et al., 1996, 1997; Martin and Lowell, 1997; Takeno et al., 1998, 1998a).

Lai et al. (1985) solved the full mass, energy and silica mass balance equations by a combination of explicit monotonised upwind central difference method and the operator splitting technique. The numerical scheme was implemented for one-dimensional problems while for two-dimensional problems, they have also used the first order rate equation of Rimstidt and Barnes (1980) for the reaction term. Their numerical model was used for theoretical studies of silica deposition in a single fracture. They also applied their model to study the temperature and pressure behavior as well as the silica transients in the Ellidaar geothermal field in Iceland.

Itoi et al. (1985, 1986, 1986a, 1987) studied the isothermal one dimension and radial transport of silica in porous medium. They solved the silica conservation equation using a finite difference method. They represented the deposition rate by several alternative kinetic models.

Verma and Pruess (1988) used a numerical model to study the dissolution and precipitation of quartz silica near a high-level nuclear waste emplaced in liquid-saturated hydrothermal system. They employed a modified version of the MULKOM simulator, which included the rate equation of Ramstidt and Barnes (1980). They have studied both the canister problem and the repository-wide thermal convection problem and compared the results of thermo-hydrological conditions with and without inclusion of silica redistribution effects. They found that silica redistribution in water saturated condition does not have a sizable effect on host rocks canister temperature, pressure or flow velocities.

Wells and Ghiorso (1991) have calculated the rate of decrease in porosity and permeability in a porous medium as fluid flowed at constant rate against a uniform geothermal gradient. They solved one-dimension rate equation using a finite difference method, and applied to problems of silica mass transfer in mid ocean ridge hydrothermal systems. To represent the deposition of quartz, they used the general kinetics rate equation of Lasaga (1984).

Malate and O'Sullivan (1992) presented a mathematical model to describe silica transport and deposition in porous medium. In particular, they derived analytical solutions for the idealized problem of isothermal constant rate and variable rate injection into a packed column or a one-dimensional channel. They used several forms of kinetic models of silica deposition and solved the problem using the method of characteristics. The changes in porosity and permeability resulting from deposition were included in their models.

Malate and O'Sullivan (1992a) performed the problem of transport and deposition of silica in non-isothermal flow, either in porous medium or single fracture. Same as the previous work, they obtained analytic solutions for both the one-dimensional problem of constant rate injection into channel or packed column and radially symmetric problem of the flow away from a reinjection well. They represented silica deposition by a rate equation of Rimstidt and Barnes (1980). The model was applied to some field data from the Otake geothermal field, Japan.

Malate and O'Sullivan (1993) extended to analyze silica deposition effects into a uniform layer from a well that produces radially symmetric flow. The mathematical model developed also uses the standard chemical transport-reaction term representing the deposition of silica. The first order rate equation of Rimstidt and Barnes (1980) was used to present silica deposition. The model derived was applied to simulate the changes in injectivity of some reinjection wells in the Tongonan geothermal field in Philippines.

Lowell et al. (1993) performed similar calculations with Wells and Ghiorso (1991) but considered flow in discrete fractures and accounted for heat transfer between up-welling fluid and adjacent rock as well as the effect of pressure on silica solubility. They showed that decrease in permeability resulting from silica precipitation occurred about an order of magnitude more slowly than for thermal expansion.

Steefel and Lasaga (1994) developed a numerical model for computing coupled multi-component chemical reactions, multi-species chemical transport, hydrodynamics flow, and heat transfer. The model was solved simultaneously using a finite difference method for multi-component reaction and solute transport in one and two dimensions. They questioned the validity of maintaining equilibrium between dissolved silica, and quartz on the fracture walls as assumed by Lowell et al. (1993). Steefel and Lasaga showed, in fact that the flow rate is an important parameter in controlling the amount of super-saturation of dissolved silica, and argued that silica reaction kinetics need to be considered in order to correctly model permeability reduction by silica precipitation. Steefel and Lasaga (1994) also considered thermal convection in an initially homogeneous, porous box heated from below in which permeability was affected by kinetically controlled silica precipitation/dissolution. They showed that the reduction in permeability by precipitation caused the flow to be more diffusive, whereas mineral dissolution caused the flow to be more focused.

White (1995) presented an algorithm for the transport of reacting chemical species in multi-phase fluid systems such as those found in geothermal reservoirs. This algorithm has been incorporated into the geothermal simulator TOUGH2 (Pruess, 1991). He applied it to several example problems of geothermal reservoirs and considered similar problems that presented by Steefel and Lasaga (1994).

In recent work on effect of thermoelasticity, Martin and Lowell (1997) developed a numerical model for the evolution of fracture permeability resulting from combined effects of thermoelastic stresses and precipitation of silica as high-temperature, reactive fluid traverses temperature and pressure gradient. They validated the model by comparing the results with those from Moore et al. (1983), on cylindrical granite cores. They obtained that the model results show a rapid initial decrease in permeability resulting from thermoelastic stresses, followed by a further decrease resulting from silica precipitation. They suggested that disagreement between the model and laboratory data caused complication such as reaction kinetics, precipitation of other minerals and nonhomogenous crack distributions.

3. MODEL FORMULATION

In order to gain a better quantitative understanding of the silica deposition in porous medium, and to aid analysis of future wastewater injection effort, a numerical simulator has been developed, that can model the evolution of permeability and porosity.

In this section, details of mathematical and numerical formulation of the simulator are given. The results of simulation of several laboratory scale experiments will be presented in Section 4.

3.1 Assumptions

The numerical simulator has been developed for the purpose of modeling single-phase two-components (water and silica) flow in a geothermal system. This code is based on the general finite difference method.

In the present formulation, the system is assumed to be composed of two mass components, water and silica. Each component flows responding to pressure and gravitational forces according to the Darcy's law. As transport of two mass components occurs by advection, it is assumed that water and silica are in a local chemical and thermal equilibrium.

3.2 Governing Equation

In a non-isothermal system, two mass balance equations and one energy conservation equation are needed for fully describing the system. The following summarizes the governing transport equations. The mass continuity equation of water can be expressed as

$$\nabla \cdot \left[\frac{k\rho_w}{\mu_w} (\nabla p - \rho_w g \nabla Z) \right] = \frac{\partial}{\partial t} (\phi \rho_w) + \bar{q}_w \tag{6}$$

where ϕ is the porosity, ρ_w is the water density, $\bar{q}_w$ is the injection rate of water per unit volume of rock. The left-hand side is the flux term, where k is the absolute permeability, μ_w is the water dynamic viscosity, p is the pressure, and g is the gravitational acceleration.

The equation for conservation of silica in porous media can be expressed as:

$$\nabla \cdot \left[\frac{k\rho_w}{\mu_w} C(\nabla p - \rho_w g \nabla Z) \right] - \nabla \cdot (\rho_w D \nabla C) = \frac{\partial}{\partial t} (\phi \rho_w C) + \bar{q}_c - R_c \phi \tag{7}$$

where C is the silica concentration, D is the diffusion coefficient, $\bar{q}_c$ is the injection rate of silica per unit rock volume, and R_c is the rate of silica reaction.

The equation for conservation of energy is given by

$$\nabla \cdot \left[\frac{k\rho_w}{\mu_w} h_w (\nabla p - \rho_w g \nabla Z) \right] - \nabla \cdot (K_T \nabla T) = \frac{\partial}{\partial t} (\phi \rho_w U_w + (1-\phi) \rho_r c_r T) + \bar{q}_h \tag{8}$$

where h_w is the water specific enthalpy, K_T is the thermal conductivity, U_w is the specific internal energy, ρ_r is the rock density, c_r is the heat capacity of the rock, T is the temperature, and $\bar{q}_h$ is the injection rate of heat per unit rock volume.

3.3 Numerical Solution Method

The finite difference method is used to discretize the flow domain into rectangular grid system. Eq. (6) may be rewritten as:

$$\nabla \cdot [\lambda_w (\nabla p - \rho_w g \nabla Z)] = \frac{\partial}{\partial t} (\phi \rho_w) + \bar{q}_w \tag{9}$$

where the water mobility λ_w is given as:

$$\lambda_w = \left(\frac{k\rho_w}{\mu_w} \right) \tag{10}$$

Then

$$\nabla \cdot [\lambda_w (\nabla p - \rho_w g \nabla Z)] = \frac{\partial}{\partial x} \left(\lambda_{wx} \frac{\partial p}{\partial x} \right) + \frac{\partial}{\partial y} \left(\lambda_{wy} \frac{\partial p}{\partial y} \right) + \frac{\partial}{\partial z} \left(\lambda_{wz} [\frac{\partial p}{\partial z} - \rho_w g \frac{\partial}{\partial z} Z)] \right) \tag{11}$$

The flow term for z direction in Eq. (11) is discretized as follows:

$$\frac{\partial}{\partial z}\left(\lambda_{wz}\frac{\partial p}{\partial z}\right)=\Delta_Z(\lambda_{wz}\Delta_Z p) \tag{12}$$

where $\Delta_Z p=\dfrac{p_{k+1}-p_k}{\Delta Z_{k+1/2}}=\dfrac{p_k-p_{k-1}}{\Delta Z_{k-1/2}}$

Multiplying Eq. (12) by the grid block volume $V_b(=\Delta Z_k A_k)$,

$$\begin{aligned}V_b\Delta_Z(\lambda_{wz}\Delta_Z p)&=\Delta_Z(\Delta Z_k A_k\lambda_{wk}\Delta_Z p)\\&=\frac{1}{\Delta Z_k}\left[(\Delta Z_k A_k\lambda_{wk}\Delta_Z p)_{k+1/2}-(\Delta Z_k A_k\lambda_{wk}\Delta_Z p)_{k-1/2}\right]\\&=TZ_{w.k+1/2}(p_{k+1}-p_k)-TZ_{w.k-1/2}(p_k-p_{k-1})\end{aligned} \tag{13}$$

where

$$TZ_{w.k\pm1/2}=\frac{\lambda_{w.k\pm1/2}A_k}{\Delta Z_{k\pm1/2}}=\left(\frac{k\rho_w}{\mu_w}\right)_{k\pm1/2}\frac{A_k}{\Delta Z_{k\pm1/2}}$$

For the gravity term of Eq. (11):

$$\frac{\partial}{\partial z}\left(\lambda_{wz}\rho_w g\frac{\partial}{\partial z}Z\right)=\Delta_Z\left(\lambda_{wz}\rho_w g\Delta_Z Z\right) \tag{14}$$

Multiplying Eq. (12) by the grid block volume $V_b(=\Delta Z_k A_k)$,

$$\begin{aligned}V_b\Delta_Z\left(\lambda_{wz}\rho_w g\nabla Z\right)=&TZ_{w.k+1/2}\rho_{w.k+1/2}g(Z_{k+1}-Z_k)\\&-TZ_{w.k-1/2}\rho_{w.k-1/2}g(Z_k-Z_{k-1})\end{aligned} \tag{15}$$

Then, a discretized expression for the flux term given by Eq. (11) is obtained by the first order finite difference approximation in space and multiplication of the bulk volume V_b.

$$\begin{aligned}&V_b\times\nabla\cdot[\lambda_w(\nabla p-\rho_w g\nabla Z)]\\&=\Delta_x[TX_w\Delta_x p]+\Delta_y[TY_w\Delta_y p]\\&\quad+\Delta_z[TZ_w\Delta_z p-TZ_w\rho_w g\Delta_z Z]\\&=TX_{w.i-1/2,j,k}p_{i-1,j,k}\\&\quad-(TX_{w.i-1/2,j,k}+TX_{w.i+1/2,j,k})p_{i,j,k}\\&\quad+TX_{w.i+1/2,j,k}p_{i+1,j,k}+TY_{w.i,j-1/2,k}p_{i,j-1,k}\\&\quad-(TY_{w.i,j-1/2,k}+TY_{w.i,j+1/2,k})p_{i,j,k}\\&\quad+TY_{w.i,j+1/2,k}p_{i,j+1,k}+TZ_{w.i,j,k-1/2}p_{i,j,k-1}\\&\quad-(TZ_{w.i,j,k-1/2}+TZ_{w.i,j,k+1/2})p_{i,j,k}\\&\quad+TZ_{w.i,j,k+1/2}p_{i,j,k+1}\\&\quad+TZ_{w.i,j,k-1/2}\rho_{w.i,j,k-1/2}g(Z_{i,j,k}-Z_{i,j,k-1})\\&\quad-TZ_{w.i,j,k+1/2}\rho_{w.i,j,k+1/2}g(Z_{i,j,k+1}-Z_{i,j,k})\end{aligned} \tag{16}$$

where $TX_{w.i\pm1/2,j,k}$ is the interblock transmissibilities of water.

The discretized form of the flow term in Eq. (7) becomes:

$$\begin{aligned}&V_b\times\nabla\cdot[T_c(\nabla p-\rho_w g\nabla Z)]\\&=\Delta_x[TX_c\Delta_x p]+\Delta_y[TY_c\Delta_y p]\\&\quad+\Delta_z[TZ_c\Delta_z p-TZ_c\rho_w g\Delta_z Z]\\&=TX_{c.i-1/2,j,k}p_{i-1,j,k}\\&\quad-(TX_{c.i-1/2,j,k}+TX_{c.i+1/2,j,k})p_{i,j,k}\\&\quad+TX_{c.i+1/2,j,k}p_{i+1,j,k}\\&\quad+TY_{c.i,j-1/2,k}p_{i,j-1,k}\\&\quad-(TY_{c.i,j-1/2,k}+TY_{c.i,j+1/2,k})p_{i,j,k}\\&\quad+TY_{c.i,j+1/2,k}p_{i,j+1,k}\\&\quad+TZ_{c.i,j,k-1/2}p_{i,j,k-1}\\&\quad-(TZ_{c.i,j,k-1/2}+TZ_{c.i,j,k+1/2})p_{i,j,k}\\&\quad+TZ_{c.i,j,k+1/2}p_{i,j,k+1}\\&\quad+TZ_{c.i,j,k-1/2}\gamma_{w.i,j,k-1/2}(Z_{i,j,k}-Z_{i,j,k-1})\\&\quad-TZ_{c.i,j,k+1/2}\gamma_{w.i,j,k+1/2}(Z_{i,j,k+1}-Z_{i,j,k})\end{aligned} \tag{17}$$

where $TX_{c.i\pm1/2,j,k}$ is the interblock transmissibilities of silica.

The discretized form of the flow term in Eq. (8) becomes:

$$\begin{aligned}&V_b\times\nabla\cdot[T_h(\nabla P-\rho_w g\nabla Z)]\\&=\Delta_x[TX_h\Delta_x P]+\Delta_y[TY_h\Delta_y P]\\&\quad+\Delta_z[TZ_h\Delta_z P-TZ_h\rho_w g\Delta_z Z]\\&=TX_{h.i-1/2,j,k}P_{i-1,j,k}\\&\quad-(TX_{h.i-1/2,j,k}+TX_{h.i+1/2,j,k})P_{i,j,k}\\&\quad+TX_{h.i+1/2,j,k}P_{i+1,j,k}\\&\quad+TY_{h.i,j-1/2,k}P_{i,j-1,k}\\&\quad-(TY_{h.i,j-1/2,k}+TY_{h.i,j+1/2,k})P_{i,j,k}\\&\quad+TY_{h.i,j+1/2,k}P_{i,j+1,k}\\&\quad+TZ_{h.i,j,k-1/2}P_{i,j,k-1}\\&\quad-(TZ_{h.i,j,k-1/2}+TZ_{h.i,j,k+1/2})P_{i,j,k}\\&\quad+TZ_{h.i,j,k+1/2}P_{i,j,k+1}\\&\quad+TZ_{h.i,j,k-1/2}\rho_{w.i,j,k-1/2}g(Z_{i,j,k}-Z_{i,j,k-1})\\&\quad-TZ_{h.i,j,k+1/2}\rho_{w.i,j,k+1/2}g(Z_{i,j,k+1}-Z_{i,j,k})\end{aligned} \tag{18}$$

where $TX_{h.i\pm1/2,j,k}$ is the interblock transmissibilities of heat.

The discretized form of the thermal conductivity term in Eq. (9) becomes:

$$\begin{aligned}&V_b\times\nabla\cdot[T_t(\nabla T)]\\&=\Delta_x[TX_t\Delta_x T]+\Delta_y[TY_t\Delta_y T]+\Delta_z[TZ_t\Delta_z T]\\&=TX_{t.i-1/2,j,k}T_{i-1,j,k}\\&\quad-(TX_{t.i-1/2,j,k}+TX_{t.i+1/2,j,k})T_{i,j,k}\\&\quad+TX_{t.i+1/2,j,k}T_{i+1,j,k}\\&\quad+TY_{t.i,j-1/2,k}T_{i,j-1,k}\\&\quad-(TY_{t.i,j-1/2,k}+TY_{t.i,j+1/2,k})T_{i,j,k}\\&\quad+TY_{t.i,j+1/2,k}T_{i,j+1,k}\\&\quad+TZ_{t.i,j,k-1/2}T_{i,j,k-1}\\&\quad-(TZ_{t.i,j,k-1/2}+TZ_{t.i,j,k+1/2})T_{i,j,k}\\&\quad+TZ_{t.i,j,k+1/2}T_{i,j,k+1}\end{aligned} \tag{19}$$

where $TX_{t,i\pm1/2,j,k}$ is the interblock transmissibilities of the thermal conductivity.

The discretized form of the right hand side in Eq. (6) can be expressed as:

$$\frac{V_b}{\Delta t}\Delta_t(\phi\rho_w)+V_b\bar{q}_w=\frac{V_b}{\Delta t}\left[(\phi\rho_w)^{n+1}-(\phi\rho_w)^n\right]+q_w \quad (20)$$

The discretized form of the right hand side in Eq. (7) can be expressed as:

$$\begin{aligned}&\frac{V_b}{\Delta t}\Delta_t(\phi\rho_w C)+V_b\bar{q}_c-V_bR_c\phi=\\&\qquad\frac{V_b}{\Delta t}\left[(\phi\rho_w C)^{n+1}-(\phi\rho_w C)^n\right]+q_c-V_bR_c^{n+1}\phi\end{aligned} \quad (21)$$

The discretized form of the right hand side in Eq. (8) can be expressed as:

$$\begin{aligned}&\frac{V_b}{\Delta t}\Delta_t(\phi\rho_wU_w+(1-\phi)\rho_rC_rT)+V_b\bar{q}_h\\&\quad=\frac{V_b}{\Delta t}\left[(\phi\rho_wU_w+(1-\phi)\rho_rc_rT)^{n+1}\right.\\&\qquad\left.-(\phi\rho_wU_w+(1-\phi)\rho_rc_rT)^n\right]+q_h\end{aligned} \quad (22)$$

Time is discretized as fully implicit first-order finite difference. This ensures the numerical stability necessary for efficient simulation of multicomponent flow. The mass and energy balance equations given by Eqs. (6) through (8) may be written in a discretized form in term of the residual of each component in each grid block:

$$\begin{aligned}Fw_{i,j,k}&=\Delta_x[TX_w\Delta_x p]_{i,j,k}^{n+1}+\Delta_y[TY_w\Delta_y p]_{i,j,k}^{n+1}\\&\quad+\Delta_z[TZ_w\Delta_z p-TZ_w\rho_w g\Delta_z Z]_{i,j,k}^{n+1}\\&\quad-\frac{V_{b.i,j,k}}{\Delta t}\left[(\phi\rho_w)^{n+1}-(\phi\rho_w)^n\right]_{i,j,k}\\&\quad-(q_w)_{i,j,k}=0\end{aligned} \quad (23)$$

$$\begin{aligned}Fc_{i,j,k}&=\Delta_x[TX_c\Delta_x p]_{i,j,k}^{n+1}+\Delta_y[TY_c\Delta_y p]_{i,j,k}^{n+1}\\&\quad+\Delta_z[TZ_c\Delta_z p-TZ_c\rho_w g\Delta_z Z]_{i,j,k}^{n+1}\\&\quad-\frac{V_{b.i,j,k}}{\Delta t}\left[(\phi\rho_w C)^{n+1}-(\phi\rho_w C)^n\right]_{i,j,k}\\&\quad-(q_c)_{i,j,k}+V_{b.i,j,k}[R_c\phi]_{i,j,k}^{n+1}=0\end{aligned} \quad (24)$$

$$\begin{aligned}Fh_{i,j,k}&=\Delta_x[TX_h\Delta_x p]_{i,j,k}^{n+1}+\Delta_y[TY_h\Delta_y p]_{i,j,k}^{n+1}\\&\quad+\Delta_z[TZ_h\Delta_z p-TZ_h\rho_w g\Delta_z Z]_{i,j,k}^{n+1}\\&\quad-\Delta_x[TX_t\Delta_x T]_{i,j,k}^{n+1}+\Delta_y[TY_t\Delta_y T]_{i,j,k}^{n+1}\\&\quad+\Delta_z[TZ_t\Delta_z T]_{i,j,k}^{n+1}\\&\quad-\frac{V_{b.i,j,k}}{\Delta t}\left[(\phi\rho_wU_w+(1-\phi)\rho_rc_rT)^{n+1}\right.\\&\qquad\left.-(\phi\rho_wU_w+(1-\phi)\rho_rc_rT)^n\right]_{i,j,k}\\&\quad-(q_h)_{i,j,k}=0\end{aligned} \quad (25)$$

For a flow region discretized into N-grid blocks, the equations above represent a system of $3N$ coupled nonlinear algebraic equations. The unknowns in these equations are the $3N$ primary variables at the time level $t+\Delta t$.

The nonlinear balance equations given by Eqs. (23) – (25) are linearized using a residual-based Newton-Raphson iterative technique. The Newton-Raphson technique is very powerful technique, which has been widely used for solution of a set of non-linear equations. Denoting the vector of primary variable in each grid block as X, Eqs. (23) – (25) may be written as:

$$F(X)=0 \quad (26)$$

where F is the $3N$ vector of the component residuals. Performing a Taylor series expansion of Eq. (26) about an assumed solution, $X^{(v+1)}$, and neglecting the higher-order terms results in

$$F\left(X^{(v+1)}\right)\approx F\left(X^{(v)}\right)+\left(\frac{\partial F(X)}{\partial X}\right)^{(v)}\left(X^{(v+1)}-X^{(v)}\right) \quad (27)$$

where v is iteration level. From the requirement that the residuals at the iteration index $v+1$ must vanish, Eq. (27) leads to a system of linearized matrix equation as

$$\left[\left(\frac{\partial F(X)}{\partial X}\right)^{(v)}\right]\left[\left(X^{(v+1)}-X^{(v)}\right)\right]=\left[-F\left(X^{(v)}\right)\right] \quad (28)$$

Eq. (28) represents a linear system of $3N$ simultaneous equation. These equations may be written in a more expanded matrix form as

$$\begin{bmatrix}J_{1,1}&J_{1,2}&J_{1,3}&\cdots&J_{1,N}\\J_{2,1}&J_{2,2}&J_{2,3}&\cdots&J_{2,N}\\J_{3,1}&J_{3,2}&J_{3,3}&\cdots&J_{3,N}\\\vdots&\vdots&\vdots&\vdots&\vdots\\J_{N,1}&J_{N,2}&J_{N,3}&\cdots&J_{N,N}\end{bmatrix}\times\begin{bmatrix}\Delta X_1\\\Delta X_2\\\Delta X_3\\\vdots\\\Delta X_N\end{bmatrix}=\begin{bmatrix}-F_1\\-F_2\\-F_3\\\vdots\\-F_N\end{bmatrix} \quad (29)$$

where $[J\,]$ is the Jacobian matrix, $[\Delta X\,]$ is the vector of unknown changes in the primary variables in each grid block from previous iteration, and $[-F\,]$ is the vector of residuals of each component in each grid block.

Each of Jacobian matrix elements, $J_{i,j}$ is actually a three-by-three submatrix. The $J_{i,j}$ represent the partial derivatives of the residuals in a grid block with respect to primary variables (p, T, and C) in the element, the submatrix $J_{i,j}$ is

$$J_{i,j}=\begin{bmatrix}\frac{\partial Fw}{\partial p}&\frac{\partial Fw}{\partial C}&\frac{\partial Fw}{\partial T}\\\frac{\partial Fc}{\partial p}&\frac{\partial Fc}{\partial C}&\frac{\partial Fc}{\partial T}\\\frac{\partial Fh}{\partial p}&\frac{\partial Fh}{\partial C}&\frac{\partial Fh}{\partial T}\end{bmatrix} \quad (30)$$

The partial derivatives in Eq. (30) are calculated numerically by successively incrementing each of the primary variables. As each primary variable is incremented, all of the second variables are calculated. These are used in conjunction with the incremented primary variable to calculate a new value of F. The partial derivative is calculated by subtracting the original value of F from the incremented value, and dividing by the amount of the primary variable increment. All of the partial derivatives in Eq. (30) are evaluated at iteration level v.

The vector of unknown changes in the primary variables in Eq. (29) consists of *N* groups of three-component vectors. For each grid block the primary variables are *p*, *T*, and *C* is

$$\Delta X = \begin{bmatrix} p^{(v+1)} - p^{(v)} \\ C^{(v+1)} - C^{(v)} \\ T^{(v+1)} - T^{(v)} \end{bmatrix} \tag{31}$$

The vector of residuals in Eq. (29) also consists of *N* groups of three-component vectors, *F* in Eq. (29) is

$$-F = \begin{bmatrix} -F_w(X^{(v)}) \\ -F_c(X^{(v)}) \\ -F_h(X^{(v)}) \end{bmatrix} \tag{32}$$

In Eq. (32), each of the residuals is evaluated at iteration level *v*.

At the beginning time step, the converged values of *X* from the previous time step are used as the initial solution for the first iteration. The system of simultaneous equations is solved with a general elimination without pivoting, which uses sparse storage techniques and only stores the nonzero member of the Jacobian matrix. Iteration is continued until all residuals are reduced to a small fraction of the accumulation terms (ε).

$$\left|F(X^{(v+1)})\right| \le \varepsilon \tag{33}$$

The model employs upstream weighting to calculate the interface fluid enthalpy and concentration, harmonic weighting for intrinsic permeability, and an arithmetic average for the mass density and viscosity. For example, upstream weighting is defined by

$$C_{i+1/2} = C_i \quad \text{if flow} \quad i \text{ to } i+1 \tag{34}$$

$$C_{i+1/2} = C_{i+1} \quad \text{if flow} \quad i+1 \text{ to } i \tag{35}$$

The sign of $\left[(p_{i+1} - p_i) - \rho_w g \Delta Z\right]$ gives the direction of flow. Flow is from *i* to *i*+1 if this quantity is less than zero and vice versa.

3.5 Porosity-Permeability Changes

The specific deposit is calculated using the formula suggested by Itoi el al. (1985) as

$$S_s^{t+\Delta t} = \left(\phi_0 - \phi^{t+\Delta t}\right) \times \left(\frac{1-\phi_s}{1-\phi_0}\right)\frac{\rho_s}{\rho_r} \tag{36}$$

where ϕ_s is the porosity of quartz, and ρ_s is the density of quartz (kg/m^3). The porosity of rock that decreases as silica deposits is expressed as

$$\phi^{t+\Delta t} = \phi^t + \frac{R_c^{t+\Delta t} \times \Delta t}{\rho_s} \tag{37}$$

where ρ_s is the molar density of quartz. The change is permeability as a result of deposition/precipitation is calculated using the model derived by Weir and White (1996). The permeability is given by

$$k^{t+\Delta t} = k_0 \left(1 - \left(1 - \left(\frac{\phi^{t+\Delta t} - \phi_c}{\phi_0 - \phi_c}\right)^{1.58}\right)\right)^{0.460} \tag{38}$$

where k_0 is the initial permeability, ϕ_0 and ϕ_c are the initial porosity and a critical value of porosity at which the permeability reduces to zero, respectively.

3.6 Computational Algorithm

To begin the calculation, the grid block and rock properties should be defined. The initial and boundary conditions are then initialized. At this point, the program begins checking the flow direction and stepping time. On the first iteration, it is assumed that the primary variables, porosity and permeability are the same as the previous time step. Calculations of the fluxes, accumulation, sink/source, and reaction term follow. At this point a Newton-Raphson iteration is required in order to solve primary variable at a new time step. Each Newton-Raphson iteration consists of calculating the residual of mass and energy balance equation, and the partial derivatives of these equations with respect to the primary variable (the Jacobian matrix). This is repeated until convergence is achieved. If convergence of the Newton-Raphson iteration is achieved, the permeability and porosity of rock are updated. Then calculations continue to the next time step.

4 SIMULATION RESULTS AND DISCUSSION

The numerical model of the rate of silica deposition was applied to the experimental results obtained by Itoi et al. (1984, 1986). The experiments of an isothermal flow through packed columns (Fig. 1) were discussed in Section 2. Simulation by the model was conducted only on Run #05 and Run #38.

The model parameters used in matching the changes in flow rate, permeability, specific deposit, and pressure are listed in Tables 1 and 2. A constant discretization of 40 grids were employed in *z* direction (Fig. 2), and the rate constant of Ramstidt and Barnes (1980) was used in this calculation (Eq. (3)). The boundary conditions as constant pressure at inner and outer grid block were used. With these boundary condition, the inlet and outlet rates are

$$q_i = \frac{kA\rho_w}{\mu_w L}\left(p_{in} - p_1\right) \tag{39}$$

$$q_o = \frac{kA\rho_w}{\mu_w L}\left(p_N - p_{out}\right) \tag{40}$$

where p_{in} is the injection pressure, p_1 is the pressure at first grid block, p_N is the pressure at the end of grid block, p_{out} is the pressure at outlet, *A* is the column cross-sectional area, and *L* is the distance form the center of the outermost/ innermost grid block to the outer/inner boundary (= Δz/2).

Table 2 Data used to match Itoi's experiment

Parameter	Value
Column temperature, ^{o}C	90
Density of rock, kg/m^3	3620
Density of deposited silica, kg/m^3	2040
Length of the column, cm	50
Diameter of the column, cm	5

Itoi et al. (1984) did not establish the initial permeability. Here, it was determined by trial and error. The flow rate at initial stage of the experiment is controlled by the initial permeability. Therefore the initial permeability can be determined when the calculated flow rate fits to the measured one at this stage. The initial reaction surface area, *A*, need not be very accurate since the whole rate constant, *k*, (see Eq. (3)) is varied in order to match the calculation results to the experimental data. Itoi et al. (1985) found that the way to match the flow rate, permeability, specific deposit, and pressure was to use an artificially small inlet saturation of silica. They justify this by claiming only some of the silica is available for deposition. In this calculation we have adopted a value of the rate constant similar to their value.

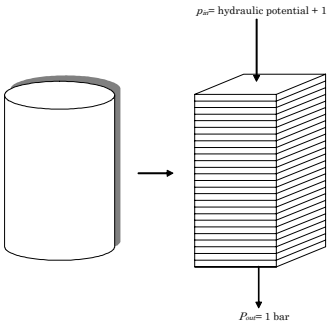

Fig. 2 Grid model of the column porous medium

4.1 Run #05

The parameters used to match in this calculation were permeability 1.464×10^{-9} m^2, rate constant k = 1.265, and porosity of silica ϕ_s = 0.932. The results of simulation are shown in Figs. 3(A), 3(B), 3(C), 4, 5, 6, and 7 for permeability, specific deposit, porosity, flow rate versus time, pressure versus distance, history of permeability versus distance, and permeability versus time, respectively.

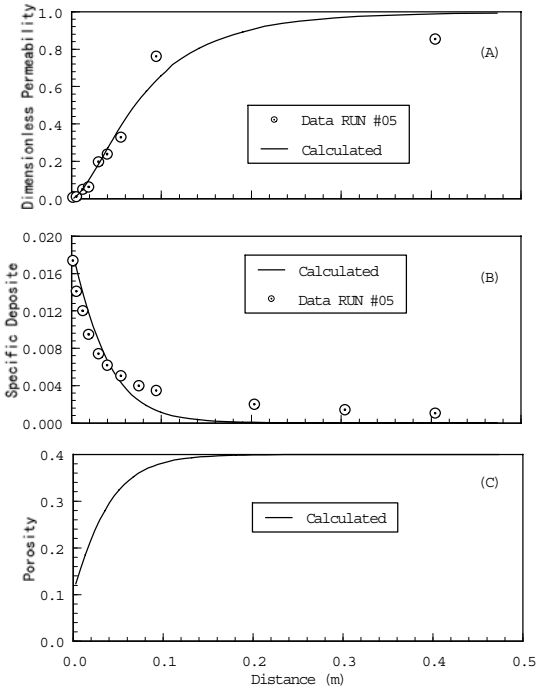

Fig. 3 Dimensionless permeability versus distance (A), specific deposit versus distance (B), and porosity versus distance (C) for Itoi's Run #05.

A good agreement found only at the distance near the inlet (Fig. 3). Figs. 5 and 6 represent the distributions of measured and calculated pressures and permeability for different time, respectively. At time = 0 minutes, the pressure curve shows linear distribution along the porous medium, since there is no silica deposition. As is expected from the permeability distribution in Fig. 6, pressure decreases with time. In particular, total decrease is mainly at place from 0 to 10 cm in the distance. The calculated permeability curve (Fig. 6) for time = 3940 minutes shows slightly higher values than the experimental data.

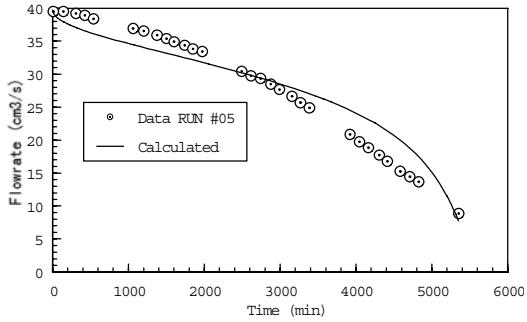

Fig. 4 Flow rate versus time for Itoi's Run #05

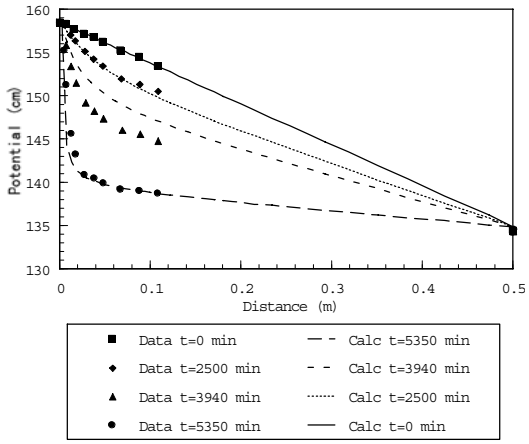

Fig. 5 Potential versus distance for Itoi's Run #05

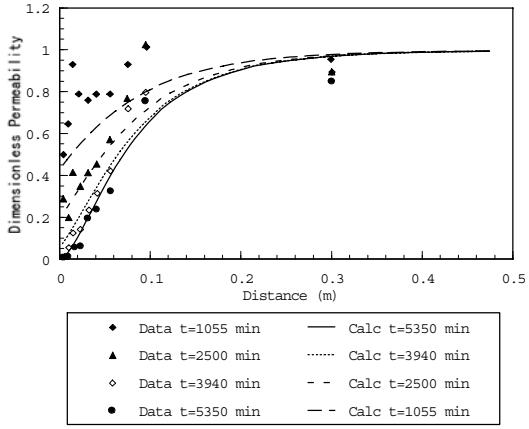

Fig. 6 History of dimensionless permeability versus distance for Itoi's Run #05

Fig. 7 compares the calculated results and the experimental permeability versus time for different distances. At early times, there is a very rapid reduction in the calculated permeability. A good match between the calculated

permeability and measured data is found at a late time for distance less than 10 cm from inlet. While at distance of 30 cm the calculated curve shows values higher than the experimental data. As seen in Fig. 4, at early time the calculated flow rate also shows lower values than measured data and higher values at late time.

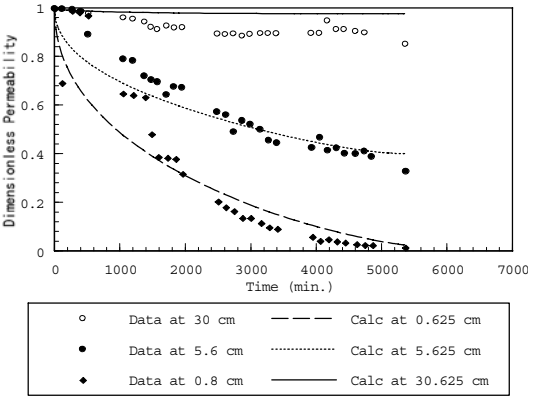

Fig. 7 Dimensionless permeability versus time for Itoi' Run #05

4.2 Run #38

The best fit to the measured data of Run #38 was achieved with a permeability 1.279×10^{-9} m^2, rate constant $k = 0.590$, and porosity of silica $\phi_s = 0.923$. The calculated results for distributions of permeability, specific deposit, and porosity are presented in Figs. 8(A), 8(B), and 8(C), respectively. The flow rate changes and pressure distribution are also shown in Figs. 9 and 10, respectively.

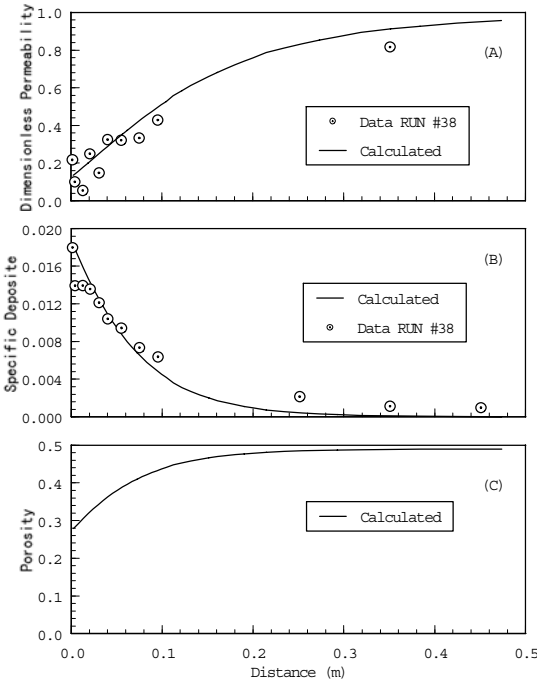

Fig. 8 Dimensionless permeability versus distance (A), specific deposit versus distance (B), and porosity versus distance (C) for Itoi's Run #38.

Same as the results of the other runs, Run #38 also shows that permeability reduction and silica deposition occurred mainly near the inlet of the column (see Figs. 8). A good agreement between the experimental and model results is seen only near the injection inlet. Fig. 9 presents the comparison of calculated and measured flow rate. The reasonable agreement between the calculation of changes in injection flow rate and the data is observed. The calculated pressure distribution matches very well with the measured pressure (Fig. 10).

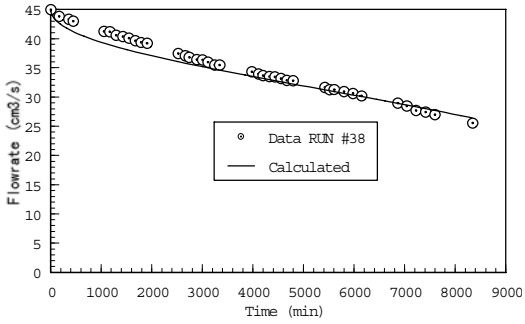

Fig. 9 Flow rate versus time for Itoi's Run #38

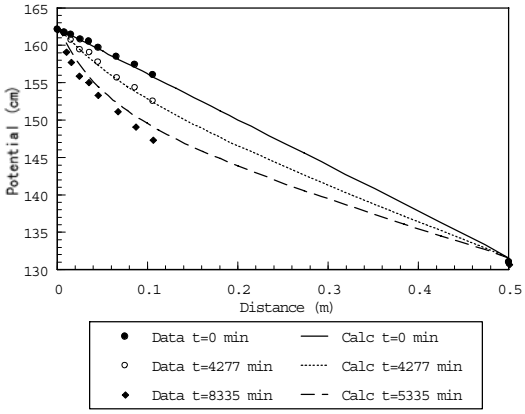

Fig. 10 Potential versus distance for Itoi's Run #38

5 CONCLUSIONS

A fully implicit numerical model, which describes the porosity and permeability decrease caused by the silica deposition in porous medium, has been used to simulate the experiments of silica deposition in geothermal reservoirs.

The numerical model of the rate silica deposition was applied to the experiments of isothermal flow through packed columns. The rate constant of Ramstidt and Barnes (1980) and an artificially small inlet saturation of silica were used to match the flow rate, permeability, specific deposit, and pressure. The poor agreement between the experimental and model results was seen far away from the inlet, for permeability and specific deposit. Silica deposition and associated permeability–porosity reduction occur mainly near the inlet.

The relationship of reaction surface area with porosity is important and should be included when modeling deposition.

ACKNOWLEDGEMENTS

This paper is a part of my Master thesis (March, 1999); for various reasons, I lost a chance to publish it earlier. I would like to express my sincere thanks to my advisor, Prof. Norio Arihara, Waseda University, Tokyo, Japan, for his valuable comments and encouragement, and for his continuous support on my research activities. Thanks also go to INPEX Foundation for providing the financial support during my study.

REFERENCES

Bohlmann, E.G., Mesmer, R.E., and Berlinski, P. (1980): Kinetics of silica deposition from simulated geothermal brines, *Society Petroleum Engineering Journal*, **Aug**., 239-248.

Bolton, E.W, Lasaga, A.C., and Rye, D.M. (1996): A Model for the kinetic control of quartz dissolution and precipitation in porous media flow with spatially variable permeability: formulation and examples of thermal convection, *Journal of Geophysical Research*, **101**, 22157-22187.

Bolton, E.W, Lasaga, A.C., and Rye, D.M. (1997): Dissolution and precipitation via forced-flux injection in a porous medium with spatially variable permeability: Kinetic control in two dimensions, *Journal of Geophysical Research*, **102**, pp. 12159-12171.

Canals, M., and Meunier, D. (1995): A model for porosity reduction in quartzite reservoir by quartz cementation, *Geochimica et Cosmochimica Acta*, **59**, 699-709.

Carroll, S., Mroczek, E., Alai, M., and Ebert, M. (1998): Amorphous silica precipitation (60 to 120 ^{o}C): Comparison of laboratory and field rates, *Geochimica et Cosmochimica Acta*, **62**, 1379-1396.

Dove, P.M. (1994): The solution kinetics of quartz in sodium chloride solutions at 25 ^{o} to 300 ^{o}C, *American Journal of Science*, **294**, 665-712.

Fleming, B.A. (1986): Kinetics of reaction between silicic acid and amorphous silica surfaces in NaCl solution. *Journal of Colloid Interface Science*, **110**, 40-64.

Itoi, R., Maekawa, H., Fukuda, M., Jinno, K., Hatanaka, K., Yokoyama, T., and Shimizu, S. (1984): Experimental study on the silica deposition in porous medium, *Geothermal Resources Council Transactions*, **8**, 301-304.

Itoi, R., Maekawa, H., Tatsuta, K., Fukuda, M., Jinno, K., Hatanaka, K., Nozaki, S., Yokoyama, T., and Shimizu, S. (1985): A mathematical model of silica deposition in a porous medium, *Geothermal Resources Council Transactions*, **9-PART II**, 337-340.

Itoi, R., Maekawa, H., Tatsuta, K., Fukuda, M., Jinno, K., Hatanaka, K., Yokoyama, T., and Shimizu, S. (1986): Numerical studies of the decrease in permeability caused by deposition of silica around an injection well, *Geothermal Resources Council Transactions*, **10**, 385-388.

Itoi, R., Maekawa, H., Tatsuta, K., Fukuda, M., Jinno, K., Hatanaka, K., Yokoyama, T., and Shimizu, S. (1986a): Study on decrease of reservoir permeability due to deposition of silica dissolved in reinjection water, *Journal of the Geothermal Research Society of Japan*, **8**, 229-241.

Itoi, R., Fukuda, M., Jinno, K., Shimizu, S., and Tomita, T. (1987): Numerical analysis of the decrease in injectivity of wells in the Otake geothermal field, Japan, *Proc. 9th NZ Geothermal Workshop*, 103-108.

Itoi, R., Fukuda, M., Jinno, K., Hirowatari, K., Shinohara, N., and Tomita, T. (1989): Long-term experiments of wastewater injection in the Otake geothermal field Japan, *Geothermics*, **18**, 153-159.

Lai, C.H., Bodvarsson, G.S., and Witherspoon P.A. (1985): Numerical studies of silica precipitation/dissolution, *Proc. 10th Stanford Geothermal Workshop*, December 22-24, 279-286.

Lowell, R.P, Cappellen, P.V., and Germanivich, L. N. (1993): Silica precipitation in fracture and the evaluation of permeability in hydrothermal upflow zones, *Science*, **260**, 192-194.

Malate, R.C.M., and O'Sullivan, M.J. (1992): Mathematical modeling of non-isothermal silica transport and deposition in a porous medium, *Geothermics*, **21**, 519-544.

Malate, R.C.M., and O'Sullivan, M.J. (1992): Mathematical modelling of silica deposition in a porous medium, *Geothermics*, **21**, 377-400.

Malate, R.C.M., and O'Sullivan, M.J. (1993): Mathematical modelling of silica deposition in Tangonan-1 reinjection wells, Philippines, *Geothermics*, **22**, 467-478.

Martin, J.T., and Lowell, R.P. (1997): On thermoelasticity and silica precipitation in hydrothermal system: Numerical modeling of laboratory experiments, *Journal of Geophysical Research*, **102**, 12095-12107.

Moore, D.E., Morrow, C.A., and Byerlee, J.D. (1983): Chemical reactions accompanying fluid flow through granite held in a temperature gradient, *Geochimica et Cosmochimica Acta*, **47**, 445-453.

Pruess, K. (1991): TOUGH2 – A general-purpose numerical simulator for multi-phase fluid and heat flow, *Rep. LBL-29400*, Lawrence Berkeley Lab., Berkeley, Calif.

Renders, P.J.N., Gammons, C.H., and Barnes, H.L. (1995): Precipitation and dissolution rate constants for cristobalite from 150 to 300 ^{o}C, *Geochimica et Cosmochimica Acta*, **59**, 77-85.

Rimstidt, J.D., and Barnes, H. L. (1980): The kinetics of silica-water reactions, *Geochimica et Cosmochimica Acta*, **44**, 1683-1699.

Rimstidt, J.D. (1997): Quartz solubility at low temperatures, *Geochimica et Cosmochimica Acta*, **61**, 2553-2558.

Steefel, C.I, and Lasaga, A.C. (1994): A coupled model for transport of multiple chemical species and kinetic precipitation/dissolution reactions with application to reactive flow in single phase hydrothermal systems, *American Journal of Science*, **294**, 529-592.

Takeno, N., Ishido, T., and Pritchettt, J. W. (1998): Numerical simulation of development of silica alteration zoning in geothermal system-Preliminary study based on kinetics reaction transport model, *Journal of Mineralogy Society Japan*, **27**, 157-166.

Takeno, N., Ishido, T., and Pritchettt, J. W. (1998a): Alteration zonation of silica minerals in a geothermal system- A numerical simulation based on reaction-transport model, *Proc. 20th NZ Geothermal Workshop*, 259-264.

Tester, J.W., Worley, W.G., Robinson, B.A., Gribsby, C.O., and Feerer, J.L. (1994): Corelating quartz dissolution kinetics in pure water from 25 to 625 ^{o}C, *Geochimica et Cosmochimica Acta*, **58**, 2407-2420.

Verma, A. and Pruess, K. (1988): Thermohydrological conditions and silica redistribution near high-level nuclear wastes emplaced in saturated geological

formations, *Journal of Geophysical Research*, **93**, 1159-1173.

Weir, G.J., and White, S. P., (1996): Surface deposition from fluid flow in a porous medium, *Transport in Porous Medium*, **25**, 79-96.

White, S.P. (1995): Multiphase nonisothermal transport of systems of reacting chemicals, *Water Resources Research*, **31**, 1761-1772.

Wells, J.T., and Ghiorso, M.S. (1991): Coupled fluid flow and reaction in mid-ocean ridge hydrothermal systems: The behavior of silica, *Geochimica et Cosmochimica Acta*, **55**, 2467-2481.